

PIV MEASUREMENTS ON A WING WITH UNIFORM BLOWING

G. Fahland¹, D. Wöllstein¹, R. Leister¹, B. Frohnappel¹ & J. Serpieri²

¹Institute of Fluid Mechanics (ISTM), Karlsruhe Institute of Technology (KIT), 76131 Karlsruhe, Germany

²Department of Mechanical and Aerospace Engineering, Politecnico di Torino, 10129 Turin, Italy

INTRODUCTION

Uniform blowing in turbulent boundary layers is a flow control scheme that offers the prospect of large friction drag reduction [7, 8]. Theoretical [4], numerical [5] and experimental investigations [1] have been conducted to investigate the influence of this control on other drag components in a more practical flow scenario than flat plate boundary layers, in particular on airfoils. One open issue in the related comparison of experimental and numerical data is the boundary condition for wall-normal blowing. While uniformity is assumed in theoretical considerations and directly enforced in numerical simulations, its experimental realization clearly has practical limitations. The present study therefore compares experimental data of the flow measured over an airfoil model with numerical data obtained with an idealized uniform blowing boundary condition.

METHODOLOGY

The airfoil model is mounted in the open jet return-type wind tunnel at ISTM [3]. The control surface is located on the airfoil’s pressure side (PS). It is made from a perforated titanium sheet metal of thickness $t = 1$ mm, hole diameter of $d_h = 60 \mu\text{m}$ and an open area ratio of $A_{\text{hole}}/A_{\text{control}} = 10\%$. It is supported by a frame that separates the control area, along the streamwise direction, in seven spanwise-extending strips. The control mass flux is monitored and regulated for each strip separately. The control intensity $c_q = v_{\text{BLC}}/U_\infty$ depends on the wall-normal velocity and the free stream (wind tunnel) velocity U_∞ . Planar Particle Image Velocimetry (PIV) measurements are conducted with a light sheet perpendicular to the airfoil’s surface as indicated in the test rig set-up shown in Fig. 1. Table 1 provides the specifications of the PIV hardware. The camera is mounted outside the free jet of the wind tunnel with a working distance of $k \approx 700$ mm. Eleven Fields of View (FOV) are examined by traversing the camera along the airfoil surface in the streamwise direction, such that the boundary layer on the PS can be investigated in the interval of $X/c = [66, 89]\%$ in the airfoil-conform coordinates. At each FOV, an image series of $n_{\text{tot}} = 410$ images is recorded alongside of analog measurements from the aerodynamic balance and pressure taps to measure integral lift and drag synchronously. The integral quantities are required to calculate the wind tunnel corrections [2], which provide the information on the infinite freestream angle of attack α_{aero} which corresponds to the geometric angle of attack α_{geom} of the experiment.

The recorded grey-scale images are investigated in a three-step process. First, each raw image is scanned for the wall position that is estimated from a brightness peak search and approximated within each FOV by a third-order polynomial fit to account for the wall curvature. The images are then

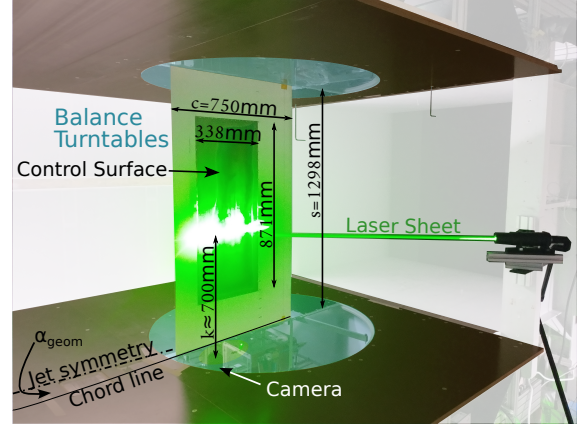


Figure 1: Test rig schematic with PIV setup

PIVLIGHT	water-based seeding	
PIVlight30	particle diameter	$d_p = 1.2 \mu\text{m}$
	response time	$t_p \approx 4.4 \mu\text{s}$
Evergreen	Wave length	532 nm
	Power	200 mJ
Nikon f/4D I	Focal length	200 mm
F-ED Nikkor	Teleplus HD 2.0X DGX	$\times 2$
PCO Edge	Sensor	sCMOS
	Resolution	2560 x 2160
2D-Target	Scaling	107.4 $\frac{\text{Pixel}}{\text{mm}}$

Table 1: PIV measurement hardware for measurements in wall-normal plane of the turbulent boundary layer

filtered using Proper Orthogonal Decomposition (POD) to reduce the light scattered from the wall [6]. In the second step, a commercially available code (*PIVview2C*) is used to conduct the PIV processing. A multigrid/multipass approach is used with a final interrogation area size of $8 \text{ px} \times 32 \text{ px}$ (wall-normal \times wall-parallel) with a 50% overlap in both directions. The corresponding datapoint step size is $4 \text{ px} \times 16 \text{ px} \hat{=} 0.037 \text{ mm} \times 0.149 \text{ mm}$ along the wall-normal and streamwise directions, respectively. In the third step, the velocity fields obtained with *PIVview2C* are treated for further processing. The velocity fields are normalized with the wind-tunnel velocity to account for low frequency ($< 1 \text{ Hz}$) wind-tunnel velocity fluctuations and ambient conditions such as density. Static pixel locking close to the wall is the most pronounced problem of the presented data despite the raw image treatment with POD. Therefore, a velocity threshold of $u/U_\infty = 3\%$ is introduced, below which an instantaneous velocity is discarded from temporal averaging. This is possible as no backflow events are expected for the present campaign. This also provides an indicator function for data quality: The number of snapshots used for temporal average n_{avg} compared to the total number of snapshots $n_{\text{tot}} = 410$ indicates threshold violation to provide information on data uncertainty.

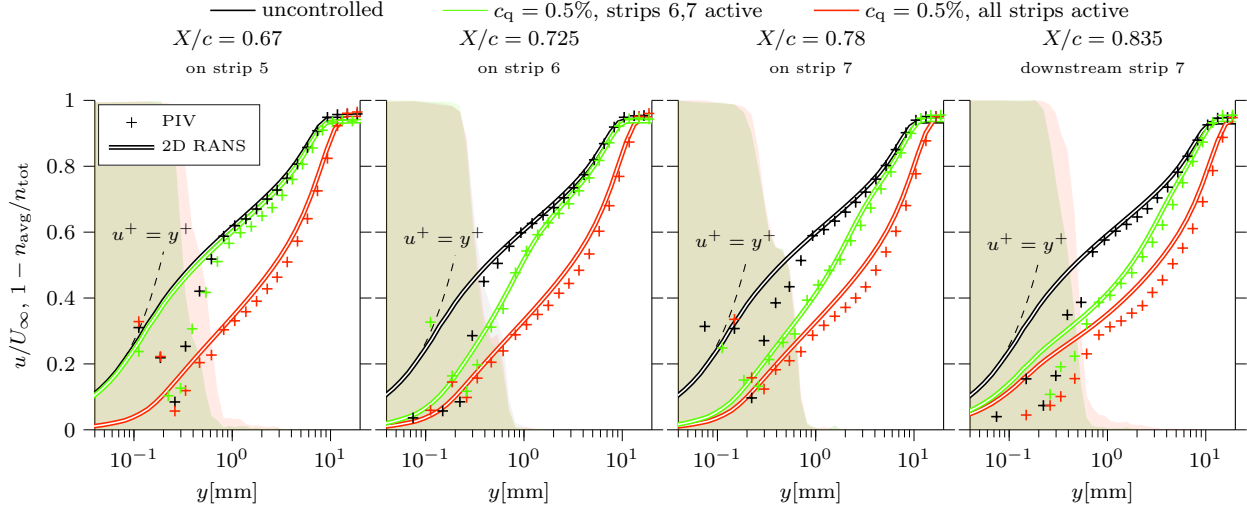


Figure 2: Time-averaged wall-parallel velocity u normalized by the wind tunnel velocity U_∞ displayed by lines and markers. Opaque fields show the ratio of excluded snapshots $1 - n_{\text{avg}}/n_{\text{tot}}$ of the average as a function of wall distance y . Opaque fields are color-coded with the respective case colors (■: uncontrolled; ■: strips 6,7 active; ■: all strips active). $\alpha_{\text{geom}} = 4^\circ$, $\alpha_{\text{aero}} = 1.09^\circ$, chord Reynolds number $Re_c = 1.5\text{Mio}$, $v_{\text{BLC}} = 15.9 \frac{\text{cm}}{\text{s}}$, $U_\infty = 31.8 \frac{\text{m}}{\text{s}}$

RESULTS

The boundary layer velocity profiles of four streamwise stations and three different configurations for a geometrical angle of attack $\alpha_{\text{geom}} = 4^\circ$ are shown in Figure 2. The uncontrolled configuration (in black) describes the case where control is completely inactive and the surface-averaged wall-normal velocity $v_{\text{BLC}} = 0$. The agreement of the boundary layer velocity profile with 2D Reynolds-Averaged Navier-Stokes (RANS) simulations at the same lift conditions (identical to the angle of attack in an infinite freestream $\alpha_{\text{aero}} = 1.09^\circ$) is good down to a wall distance of about $y \gtrsim 0.6$ mm. This coincides with the distance where the number of snapshots excluded for the temporal average ($1 - \frac{n_{\text{avg}}}{n_{\text{tot}}}$) rises abruptly, presumably due to “locking” to static wall reflections. This implies that the boundary layer conditions of the 2D numerical case and the 3D wind tunnel experiment match well and the properties of the perforated surface are close to an unaltered smooth wall. This also implies the good agreement of the integral quantities, which are not the topic of the data presented here but are required to find the 2D freestream case corresponding to the 3D experiment using wind tunnel corrections [2].

The modified boundary layer profiles (green and red curves) show the expected reduction of wall-parallel velocity due to the applied control. The case with blowing applied to all spanwise strips (+) shows that the boundary layer has already thickened significantly compared to the uncontrolled case when it reaches the area investigated by PIV. The case with partial control (+) captures the effect that the start of the control has on the boundary layer profiles. Overall, the good agreement of experimental and numerical results persists for the controlled cases. This leads to the conclusion that the discrete blowing in the experiment has a limited impact on the boundary layer development compared to the uniform blowing defined in numerical studies, at least for the close-to-zero pressure gradient present at this angle of attack. Therefore, RANS simulations with idealized homogeneous blowing boundary conditions can be used as a tool to investigate this particular flow control method.

The presentation will include more detailed data on the boundary layer measurements both for controlled and uncontrolled cases as well as further information on flow uniformity

and data quality.

REFERENCES

- [1] K. Eto, Y. Kondo, K. Fukagata, and N. Tokugawa. Assessment of Friction Drag Reduction on a Clark-Y Airfoil by Uniform Blowing. *AIAA Journal*, 57(7):2774–2782, 2019.
- [2] B. F. R. Ewald, editor. *Wind tunnel wall correction - La correction des effets de paroi en soufflerie*. Number 336 in AGARDOGRAPH. AGARD, Neuilly sur Seine, 1998. DOI.
- [3] G. Fahland. User Manual for the Göttinger Windtunnel at ISTM. User Manual V1.3.0.eng, Institute of Fluid Mechanics (ISTM), Karlsruhe Institute of Technology, Karlsruhe, Germany, 2024. doi.org/10.5445/IR/1000162981.
- [4] G. Fahland, M. Atzori, A. Frede, A. Stroh, B. Frohnäpfel, and D. Gatti. Drag Assessment for Boundary Layer Control Schemes with Mass Injection. *Flow, Turbulence and Combustion*, (Progress in Flow Control and Drag Reduction), 2023.
- [5] G. Fahland, A. Stroh, B. Frohnäpfel, M. Atzori, R. Vinuesa, P. Schlatter, and D. Gatti. Investigation of Blowing and Suction for Turbulent Flow Control on Airfoils. *AIAA Journal*, 59(11):4422–4436, July 2021. DOI 10.2514/1.J060211.
- [6] M.A. Mendez, M. Raiola, A. Masullo, S. Discetti, A. Ianiro, R. Theunissen, and J.-M. Buchlin. POD-based background removal for particle image velocimetry. *Experimental Thermal and Fluid Science*, 80:181–192, January 2017.
- [7] J. Park and H. Choi. Effects of uniform blowing or suction from a spanwise slot on a turbulent boundary layer flow. *Physics of Fluids*, 11(10):3095–3105, October 1999.
- [8] A. Stroh, Y. Hasegawa, P. Schlatter, and B. Frohnäpfel. Global effect of local skin friction drag reduction in spatially developing turbulent boundary layer. *Journal of Fluid Mechanics*, 805:303–321, October 2016.